Visualization and Interpretation of the Proper Orthogonal Decomposition of Bat Wing Kinematics

Igor V. Pivkin, Sharon Swartz and David H. Laidlaw

May 15, 2006

Abstract

Bat skeletons and their intricate musculature and nervous control have the potential to produce an enormous array of wing postures, and although only some fraction of the possibilities are realized during steady forward flight, there are no obvious guidelines to suggest optimal ways to describe this complexity. Here, we employ the Proper Orthogonal Decomposition to kinematically analyze bat flight. We demonstrate how this method can significantly reduce the dimensionality of this complex data without the need for a priori hypotheses concerning the relative importance of particular motions or anatomical landmarks.

1 Introduction

The locomotor apparatus of animals is highly complex, and is employed in spatially and temporally complex ways. The mechanical framework of a vertebrate skeleton, or even a single limb, can possess hundreds of degrees of freedom due to the dozens to hundreds of muscles active at the many relevant joints, most of which have multiple axes of rotation. The unique features of bats – their specialized skeletal anatomy, high muscular control over wing conformation, and highly deformable wing-membrane skin – yield wings that undergo large changes in 3D geometry with every wing-beat cycle, and consequently produce highly maneuverable and energetically efficient flight [1, 2, 3].

Proper Orthogonal Decomposition (POD) is a well-known technique for analyzing multidimensional data. This method essentially extracts the dominant features in space and time. It provides an orthonormal basis for representing given data, which is optimal in a least squares sense [4]. The basis is completely data dependent and no a priori assumptions of the data structure is needed. The POD basis captures more statistical variance than any other basis. By truncating the POD basis the optimal lower dimensional approximation of the data can be found. Ideally, this enhances our ability to study given data in terms of a significantly reduced number of expansion coefficients. It also helps in exploring patterns in data that may reveal some insight into the process that generates them.

2 Data Acquisition

The motion-capture data of bat flight were acquired by flying more than 20 individuals of several species through a wind tunnel [5]. Two high-speed digital cameras tracked infrared markers attached to the bat wings. After selecting video frames where the motion of the bat is close to one complete wing beat, the Peak [6] motion capture system was used to extract the coordinates of markers. Each marker has three coordinates and the representation of the bat geometry at each time frame including P markers is a N-dimensional vector, where $N = 3P$. The deformation of the bat wings during the flight can be represented as a sequence of N-dimensional vectors, where each vector corresponds to some time frame $i = 1, .., M$. We apply the POD to this sequence of vectors. Due to high wing deformations during flight, the coordinates of a few markers cannot be determined in some frames and reconstruction of these missing data is necessary.

3 The POD Method

Lets consider a sequence of M numerical or experimental observations $\vec{u}_i$, where $i = 1, ..., M$ represents time. Each observation is a vector of length N. We then look for a representation of $\vec{u}_i$ in the form

$$\vec{u}_i = \vec{\phi}_0 + \sum_{k=1}^{N} \alpha_i^k \vec{\phi}_k, \tag{1}$$

where $\vec{\phi}_0 = \frac{1}{M} \sum_{i=1}^{M} \vec{u}_i$ is a mean (time-average) of the sequence and $\vec{\phi}_k$ form the orthonormal spatial basis. The unknown vectors $\vec{\phi}_k$ and the expansion coefficients α_i^k are calculated so that the average error of a D dimensional reconstruction

$$\varepsilon_D = \frac{1}{M} \sum_{i=1}^{M} \|\vec{u}_i - (\vec{\phi}_0 + \sum_{k=1}^{D} \alpha_i^k \vec{\phi}_k)\|^2, \tag{2}$$

is minimal for all $D \leq N$. Here $\| \cdot \|^2 = (\cdot, \cdot)$ is the L^2-norm, where $(\cdot, \cdot)$ denotes the standard Euclidian inner product. Minimal ε_D implies that the lower dimensional representation of the data constructed using the first D basis vectors preserves as much information as possible.

The procedure we use to compute unknown vectors $\vec{\phi}_k$ and coefficients α_i^k consists of the following steps [4]:

1. Compute the mean of the sequence,
$$\vec{\phi}_0 = \frac{1}{M} \sum_{i=1}^{M} \vec{u}_i \tag{3}$$

2. Form the mean-subtracted sequence $\vec{v}_i$ as
$$\vec{v}_i = \vec{u}_i - \vec{\phi}_0 \tag{4}$$

3. Form $N \times M$ matrix $\mathbf{V} = [\vec{v}_1 \vec{v}_2 \cdots \vec{v}_M]$ and compute the ensemble-averaged spatial covariance matrix

$$\mathbf{C} = \frac{1}{M}\mathbf{V}\mathbf{V}^T \tag{5}$$

4. Solve the eigenvalue problem

$$\mathbf{C}\mathbf{\Phi} = \mathbf{\Lambda}\mathbf{\Phi} \tag{6}$$

5. The POD basis vector $\vec{\phi}_k$ can be recovered as a k-th column of matrix $\Phi = [\vec{\phi}_1 \vec{\phi}_2 \cdots \vec{\phi}_N]$. The expansion coefficients α_i^k can be computed as

$$\alpha_i^k = (\vec{v}_i, \vec{\phi}_k) \tag{7}$$

The size of matrix $\mathbf{V}$ can be very large in applications and often prohibitive for explicit construction due to computer memory limitations. In such cases, the POD can be obtained using the snapshot method described in [7]. In the present study, the size of $\mathbf{V}$ is quite small and we employ the direct method, based on eigenvalue decomposition of the covariance matrix $\mathbf{C}$ defined by equation (5). $\mathbf{C}$ is a real, symmetric N by N matrix with non-negative eigenvalues which are the entries of the diagonal matrix $\mathbf{\Lambda}$. The columns of matrix $\mathbf{\Phi}$ (eigenvectors) are often called POD modes. Each eigenvalue λ_k represents the variance of data captured by mode $\vec{\phi}_k$. The total variance of the entire sequence of observations is equal to the sum of eigenvalues, $\sum_{k=1}^{N} \lambda_k$. The eigenvalues can be ordered naturally according the the amount of variance contained in their respective direction,

$$\lambda_1 \geq \lambda_2 \geq ... \geq \lambda_N \geq 0. \tag{8}$$

The relative importance of the k-th mode can be measured as a contribution to the entire data set as

$$E_k = \frac{\lambda_k}{\sum_{k=1}^{N} \lambda_k}. \tag{9}$$

The number of the terms, D, in a reduced dimensional approximation

$$\vec{u}_i^D = \vec{\phi}_0 + \sum_{k=1}^{D} \alpha_i^k \vec{\phi}_k \tag{10}$$

is often chosen so that expansion (10) retains some given fraction of the variance of the original multidimensional data set.

4 Missing Data Reconstruction

The construction of the POD described in section 3 assumes that given data is complete. Experimental data is often incomplete and values of some points at times may be missing. The procedure proposed in [8] completes the missing data iteratively. It starts from the average value at missing data location

Figure 1: The mean position of the bat wings.

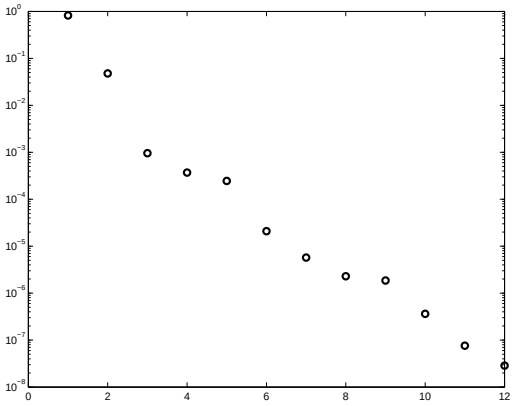

Figure 2: POD spectrum (eigenvalues) for the vertical components of the motion.

as the initial guess for the unknowns. Next, the POD basis is constructed as described in section 3. The low dimensional representation (10) with some fixed small number of modes D is constructed. The missing data is repaired with values obtained from the low dimensional representation. The improved approximation to the POD basis is constructed. The process is repeated until the basis converges.

The method was tested using the following procedure. 10-20 percent of data points were randomly removed and later reconstructed using iterative procedure. The error of the reconstruction was computed using the original data and for the data considered here was found to be of the order of 1-2 percent which is comparable to the error introduced by motion capture technique used in experiment. The error was defined as a Euclidian distance from reconstructed marker position to the original position, normalized by the wingspan of the bat model.

5 Results

In the next two sections we consider the flight of the *Pteropus Policephalus*, the grey headed flying fox (800-900 g). There are 160 frames which describe one complete wing beat during the steady forward flight. For each frame the wings geometry is represented by a vector of the three-dimensional coordinates of 27 markers.

5.1 Vertical modes

Lets first consider the vertical modes which are relatively easy to visualize and interpret. We use them here for illustration purposes. The full POD decomposition of the wings motion will be presented in the

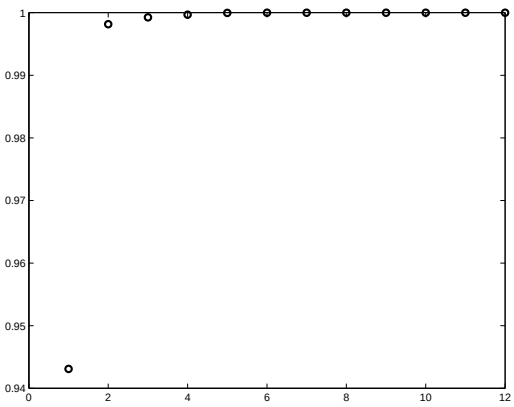

Figure 3: Accumulated variance as a function of number of modes, D, used in the low dimensional reconstruction of the vertical motion of markers.

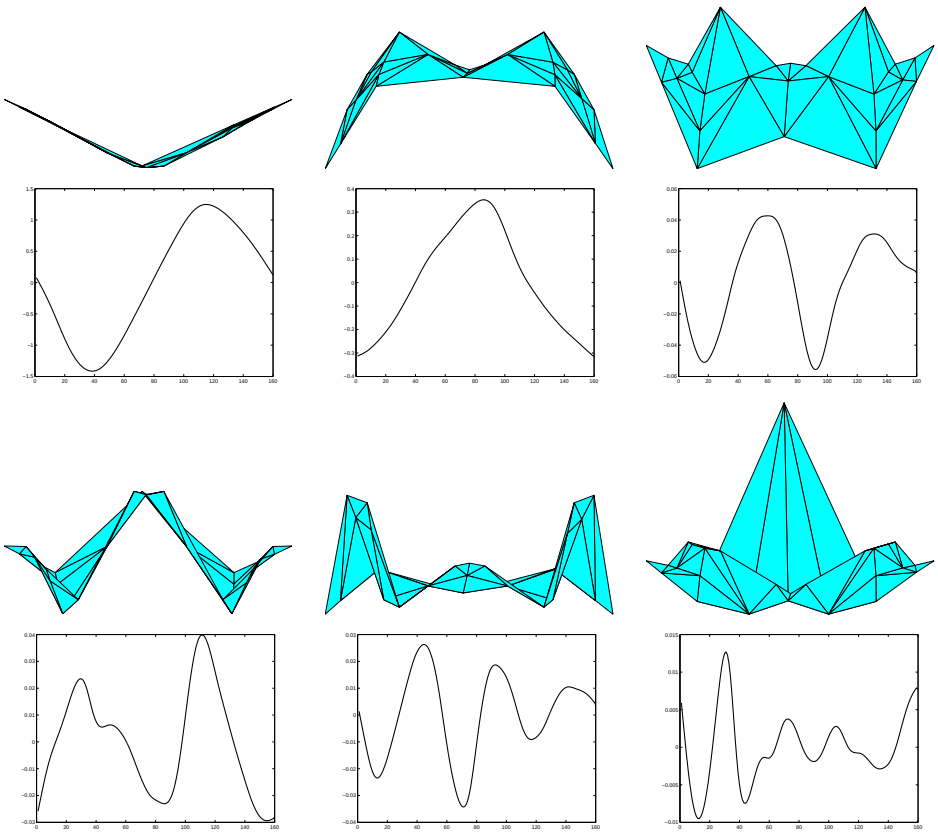

Figure 4: The geometry of the first six vertical POD modes and corresponding expansion coefficients. The modes are ordered from left to right and top to bottom.

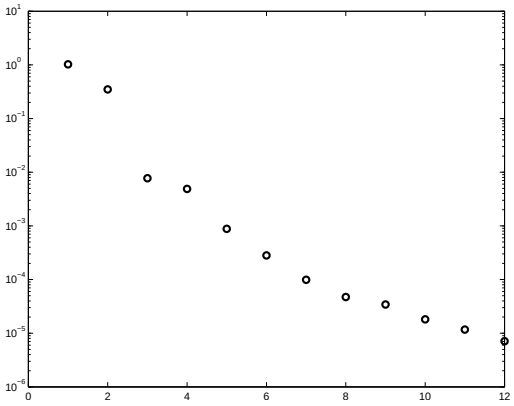

Figure 5: POD spectrum for the 3D motion of the markers.

following section.

In the lab frame of reference the vertical direction is aligned with z-axis. Here we compute the POD of the variation of the z-coordinates of the markers. In Figure 1 we plot the mean (time-average) position of the bat wings, $\vec{\phi}_0$, defined by equation (3). After subtracting the mean we solve the eigenvalue problem as described in section 3. The first twelve eigenvalues are shown in Figure 2; the eigenvalues decrease significantly with the mode index k. In Figure 3 we plot the variance captured by the low dimensional approximation given by equation (10) with different number of modes D. We note that the first mode captures more than 94% of the total variance of the data, while approximation with only two modes ($D = 2$) retains more than 99%. The first six modes $\vec{\phi}_k$ ($k = 1, ..., 6$) and the evolution of the corresponding expansion coefficients α_i^k are shown in Figure 4. The vertical motion of the markers can be reconstructed as a linear combination of the mean position, $\vec{\phi}_0$, and the modes, $\vec{\phi}_k$, multiplied by the time-varying coefficients α_i^k. The geometry of the modes can be used to explain the contribution of each mode to the total motion. The first mode captures the flapping of almost flat wings, similar to the motion of the butterfly wings during the flight. This is the most significant mode with the largest values of the expansion coefficient. The second, fourth and fifth modes capture the bending of the wings at different locations. The third mode describes the head-tail tilt, while the sixth mode corresponds to the tail motion. The contribution of mode $\vec{\phi}_k$ at time i is given by the value of the corresponding expansion coefficient α_i^k.

5.2 3D modes

In this section we consider POD of the full three-dimensional motion of the markers. In Figures 5 and 6, we plot the POD spectrum (eigenvalues) and the variance captured by the reduced dimensional expansion, respectively. Similar to the results obtained in the previous section, only few modes are required to retain significant parts of the total variance of the data.

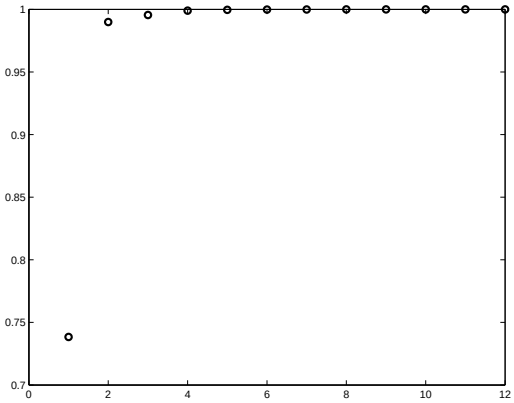

Figure 6: Accumulated variance as a function of number of modes, D, used in the low dimensional reconstruction of the 3D motion of the markers.

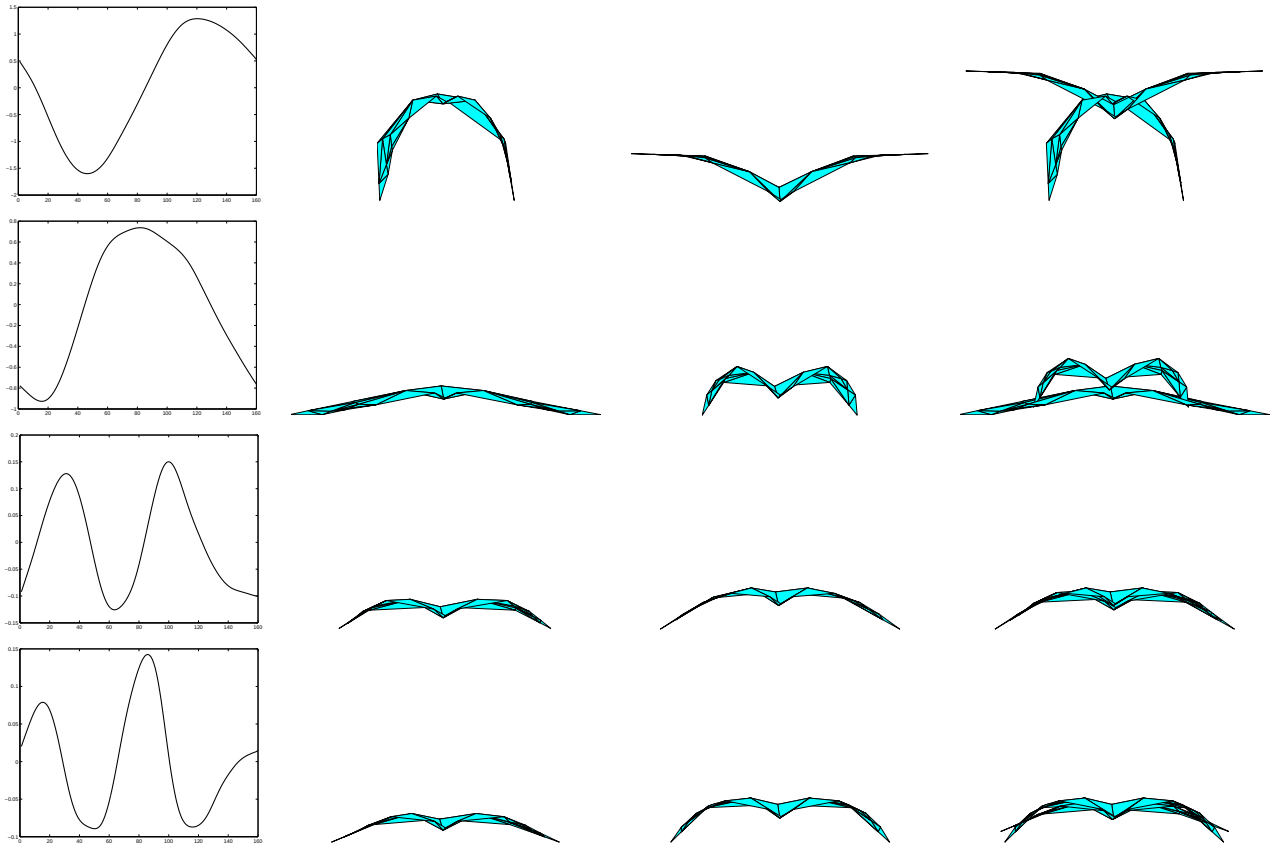

Figure 7: Expansion coefficients and mode contributions for the minimum, maximum and both values of the corresponding expansion coefficients for the first four modes.

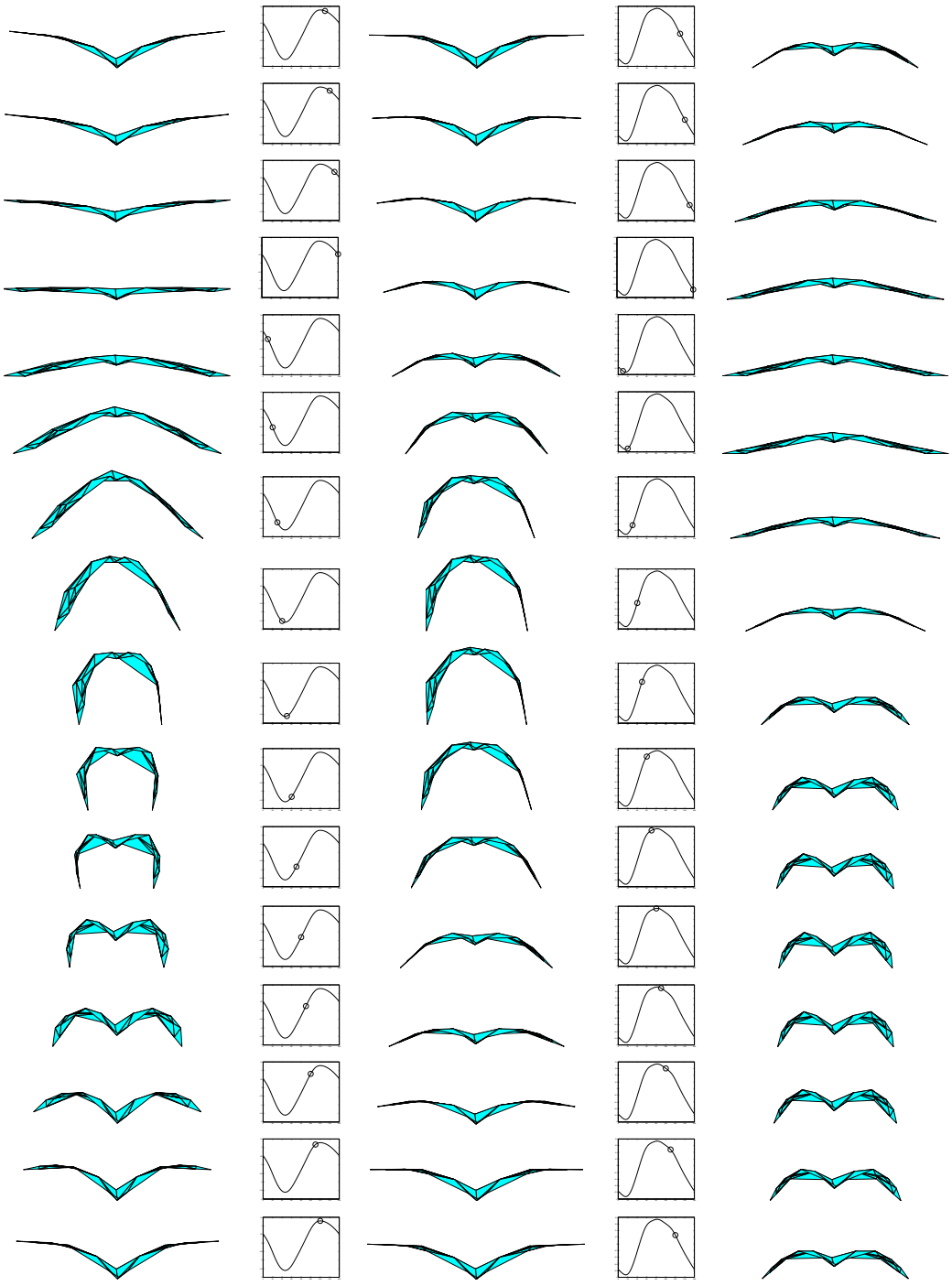

Figure 8: Full 3D motion of the bat wings, the values of the expansion coefficients and the contributions of the first and second modes at different time moments during the wing beat.

While the complexity of calculating the POD of the full three-dimensional data is essentially the same as of the vertical data, the visualization and interpretation of the POD modes are more difficult due to the large distortions of the geometry of the modes. The time-dependent contribution of mode $\vec{\phi}_k$ to the motion of the wings can be obtained using approximation (10) with all expansion coefficients except α_i^k, $i = 1, .., M$ set to zero, i.e. $\vec{\phi}_0 + \alpha_i^k \vec{\phi}_k$. By considering time frames when the expansion coefficient takes the maximum or minimum values during the wing beat we evaluate the extreme contributions of the mode to the deformation of the wings. In Figure 7 we plot the evolution of the first four expansion coefficients and the extreme contributions of the corresponding modes. The maximum absolute value of the third expansion coefficient is about 100 times smaller than that of the first expansion coefficient. The first two modes capture the most significant components of the motion. In Figure 8 we plot the values of the expansion coefficients and the contributions of the first and second modes at different time moments during the wing beat. Similar to the case considered in previous section, the first mode captures the up and down motion of almost flat wings, while the second mode represents wing bending. The upstroke and downstroke parts of the wing's motion can be readily distinguished from the time evolution of the first mode coefficient. Specifically, the starts of upstroke and downstroke phases correspond to the extrema of the first expansion coefficient. The contribution of the second mode can be interpreted as a variation of the area of the wings. During the upstroke the wings are bent to minimize negative lift, while during the downstroke the wings are flattened to increase positive lift.

5.3 Consistency of the POD modes

In this section we consider the flight of the *Chalinolobus morio*, the chocolate wattled bat (8-10 g). The wings geometry is represented by the coordinates of the 20 markers. There are 49 frames which describe one complete wing beat during the steady forward flight.

The computed POD modes were found to be similar to the modes obtained in previous sections. The first mode captured the motion of almost flat wings, while the next few modes captured the bending of the wings at different locations. In figure 9 we show the evolution of the first four expansion coefficients and the extreme contributions of the corresponding modes.

6 Visualization System

We developed a visualization system to interactively explore the POD modes of the full three dimensional motion of the bat wings. The program is based on the VRG3D framework developed at Brown University.

Our visualization tool produces a three-dimensional motion of the wings of two bat models from the pre-computed POD decompositions (see figure 10). The user interface consist of a keyboard and a mouse. The user can access the menu, grab the models, rotate them and place each of them in a preferred location

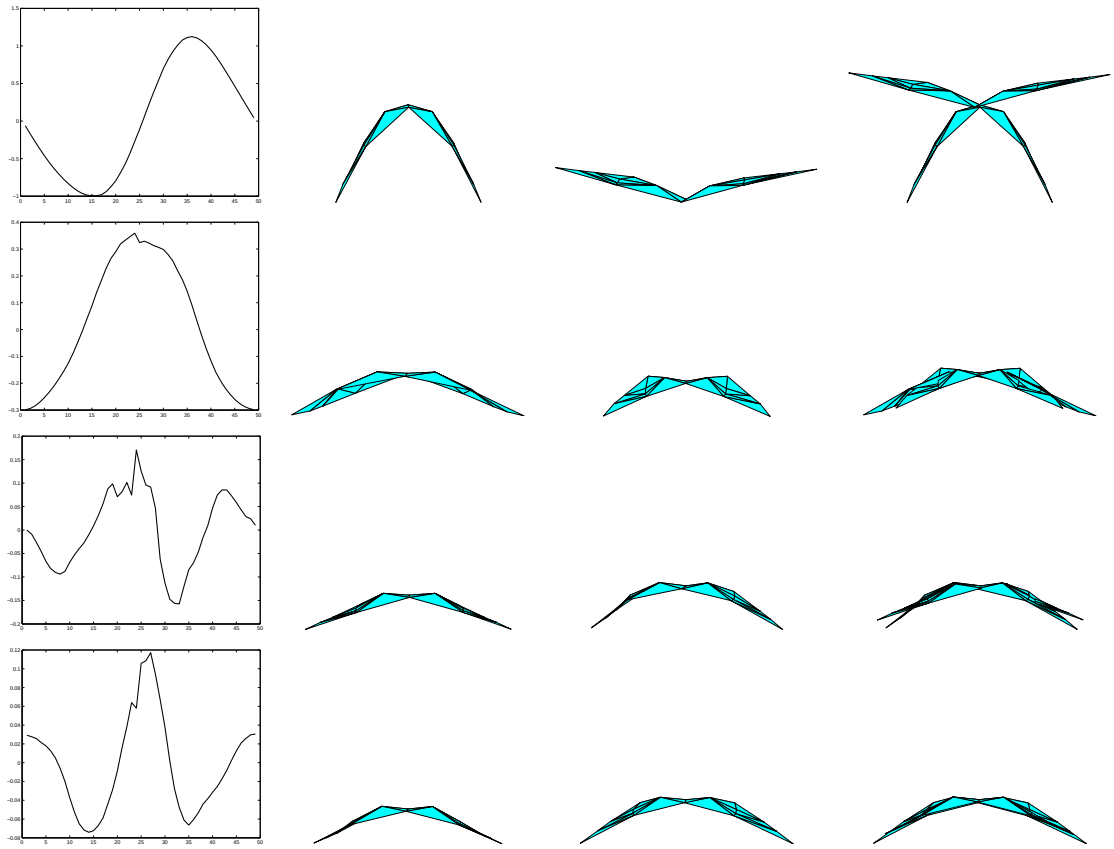

Figure 9: Chalinolobus morio bat: Expansion coefficients and mode contributions for the minimum, maximum and both values of the corresponding expansion coefficients for the first four modes.

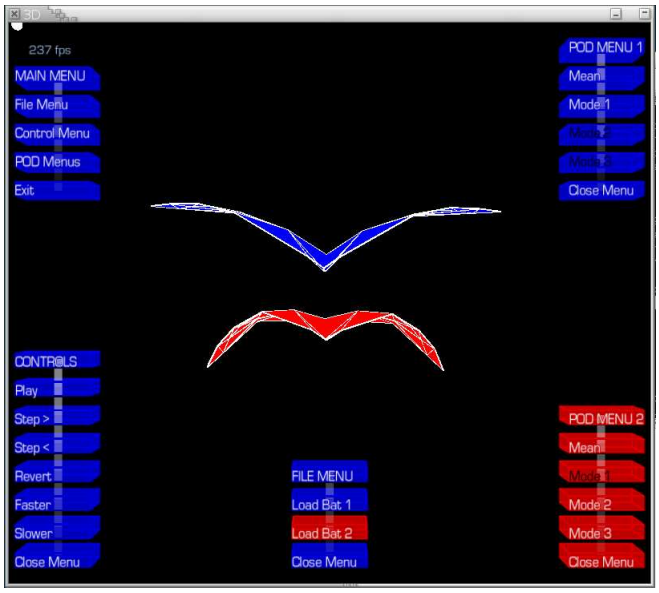

Figure 10: (in color) A screen shot from the visualization system. Two models are animated based on the different combinations of the POD modes in the low dimensional approximation.

in space. The menu provides convenient access to timestepping and speed controls, which are essential in being able to effectively and thoroughly control the animation. Using the menu, the user can interactively explore the contributions of individual, as well as different combinations, of the POD modes. For each model the user can specify what modes should be included in the low dimensional representation given by equation (10).

The visualization system was evaluated by a scientific user and received positive feedback. The user pointed out that the choice of colors for visualization of menus and the bat models was not the best. As a result, the menu button labels were difficult to read. The user suggested adding more features to the current visualization, such as traces of markers in space and finer controls of the animation of the models (phase shift between the models, number of periods to be animated). These features can be implemented in the future.

7 Summary

We have presented an application of the Proper Orthogonal Decomposition to bat wing kinematics. The complex three-dimensional motion of the wings was represented as a linear combination of simpler motions described by the POD modes. Results of preliminary studies show that POD modes are consistent between bats of different species. The visualization tool was developed to explore the contribution of individual POD modes. It was found that some of them have an intuitive interpretation.

References

[1] E.F. Stockwell. Morphology and flight manoeuvrability in new world leaf-nosed bats (chiroptera : Phyllostomidae). *Journal of Zoology*, 254:505–514, 2001.

[2] C.C. Voigt and Y. Winter. Energetic cost of hovering flight in nectar-feeding bats (phyllostomidae : Glossophaginae) and its scaling in moths, birds and bats. *Journal of Comparative Physiology B – Biochemical Systemic and Environmental Physiology*, 169(1):38–48, 1999.

[3] Y. Winter, C. Voigt, and O. Von Helversen. Gas exchange during hovering flight in a nectar-feeding bat glossophaga soricina. *Journal of Experimental Biology*, 201(2):237–244, 1998.

[4] M. Kirby. *Geometric data analysis : an empirical approach to dimensionality reduction and the study of patterns*. Wiley, New York, 2001.

[5] S. Swartz, K. Bishop, and M.F. Ismael-Aguirre. Dynamic complexity of wing form in bats: implications for flight performance. In *Functional and evolutionary ecology of bats*. Oxford Press, 2006.

[6] Peak performance, http://www.peakperform.com.

[7] L. Sirovich and M. Kirby. Low-dimensional procedure for the characterization of human faces. *Journal of the Optical Society of America a-Optics Image Science and Vision*, 4(3):519–524, 1987.

[8] R. Everson and L. Sirovich. Karhunen-loeve procedure for gappy data. *Journal of the Optical Society of America a-Optics Image Science and Vision*, 12(8):1657–1664, 1995.